Supporting Information

Uniform and size-tunable dasatinib nanoemulsions synthesized by a high-throughput microreactor for enhanced temperature stability

Authors: Su Wang [a, b], Chao Li [a], Jiaxiang Zhang [a], Kaixuan Ma [b], Wanyao Zhang [b], Yan Gao [b], Xue Li [c], Jingsheng Zhang [c], Liang Guo [c], Yingying Nie [a], Yuguang Li [d], Ruiyan Sun [a], Ning Zhu [a, e], Wei He [a], Shuangfei Zhao [a, *], Kai Guo [a, e, *]

[a] College of Biotechnology and Pharmaceutical Engineering, Nanjing Tech University, Nanjing 211816, China

[b] Tianhua Institute of Chemical Machinery & Automation Co., Ltd, Lanzhou 215128, China

[c] Sinopec Beijing Research Institute of Chemical Industry, Beijing 100029, China

[d] Institute of Nanjing Advanced Biomaterials & Processing Equipment, Nanjing 211299, China

[e] State Key Laboratory of Materials-Oriented Chemical Engineering, Nanjing Tech University, Nanjing 211816, China

*Corresponding Author: Kai Guo − College of Biotechnology and Pharmaceutical Engineering and State Key Laboratory of Materials-Oriented Chemical Engineering, Nanjing Tech University, Nanjing 211816, China; Email: guok@njtech.edu.cn; sfzhao@njtech.edu.cn.

Table of contents

Supporting Information 1: Experimental methods

SI1.1 Materials

In this study, dasatinib (98% purity, Shanghai Macklin Biochemical Co., Ltd.) served as the raw material for nanoemulsion preparation. The oil phases comprised oleic acid (90% purity, Saen Chemical Technology (Shanghai) Co., Ltd.), ethyl oleate (99% purity, Shanghai Aladdin Biochemical Technology Co., Ltd.), triacetin (98.5% purity, Shanghai Macklin Biochemical Co., Ltd.), and epoxidized soybean oil (99% purity, Shanghai Aladdin Biochemical Technology Co., Ltd.). Ethylene glycol (99% purity, Saen Chemical Technology (Shanghai) Co., Ltd.), glycerol (99.5% purity, Shanghai Bide Pharmaceutical Technology Co., Ltd.), and ethanol (99.5% purity, Shanghai Meiruier Biochemical Technology Co., Ltd.) acted as co-emulsifiers. Polyoxyethylene hydrogenated castor oil (98% purity, Beijing Huawei Ruike Chemical Co., Ltd.) and Tween 20 (98% purity, Shanghai Dibai Biotechnology Co., Ltd.) were used as emulsifiers.

SI 1.2 Preparation of Dasatinib nanoemulsion by batch reactor

Dasatinib nanoemulsion was prepared using a batch reactor, and it was compared with the products obtained by microreactors to demonstrate the superiority of the microreactor method. In this method, the optimal system for preparing nanoemulsions is determined by referring to the ternary phase diagram and drug solubility measurements of Dasatinib [1]. The concentration of Dasatinib was determined as 200μg/mL, and oleic acid, polyoxyethylene hydrogenated castor oil and ethanol were used as oil phase, emulsifier and co-emulsifier respectively. In the experiment, firstly, oleic acid, polyoxyethylene hydrogenated castor oil and ethanol were mixed at a ratio of 1:6:3 to form a mixed oil phase. Then, Dasatinib raw material was added to the mixed oil phase. Finally, the mixed oil phase and ultrapure water was mixed and stirred using a magnetic stirrer at a speed of 1000rpm to obtain the Dasatinib nanoemulsion.

SI 1.3 Preparation of Dasatinib nanoemulsion by microreactors

Generally speaking, an ideal nanoemulsion formulation is supposed to form stable small droplets. In traditional nanoemulsion laboratory preparation methods, the beaker is coupled with magnetic stirring to enhance the emulsification process. Due to the small size effect, microreactors have potential advantages in the preparation of nanoemulsion [2, 3]. In this study, a high throughput microreactor with triangular-notched rectangular baffle (TNRB) was used to enhance the Dasatinib nanoemulsion formulation processes aiming to reduce the size and size distribution of nanoemulsions. Previous literature has demonstrated the superiority of this baffle in enhancing liquid-liquid homogeneous mixing and heat transfer [4]. However, its role in liquid-liquid two-phase flow systems such as the preparation of nanoemulsions has not yet been elucidated. Additionally, Dasatinib nanoemulsion processes in the commercial microreactor were also conducted to

compare with this high throughput microreactor.

The high throughput microreactor preparation system for nanoemulsions was shown in Fig. S1. In this system, the experimental device consists of two injection pumps, two syringes, high throughput microreactor, a collection beaker, connecting pipes, and connectors, etc. The high throughput microreactor with TNRB was designed based on our previous work with the optimal baffle tilt angle of 120°, the baffle notch angle of 40°, the baffle thickness of 1mm and the baffle number of 8 [4]. Furthermore, the high throughput microreactor with TNRB was manufactured using 3D printing technology. The inner diameter of the commercial microreactor is 1mm, while that of the high throughput microreactor is 10mm. A larger microreactor scale will be beneficial for improving the preparation throughput of nanoemulsions. This paper will demonstrate the feasibility of extending the scale of the microreactor while enhancing the emulsification process. In the experiment, oil phase, emulsifier and co-emulsifier were firstly mixed as the mixed oil phase, and ultrapure water was used as the antisolvent. The mixed oil phase and ultrapure water were driven by the two injection pumps with different flow rates. They were mixed and emulsified in the microreactors, and were collected into the collection beaker. And finally they were subjected to particle size and morphology analysis tests.

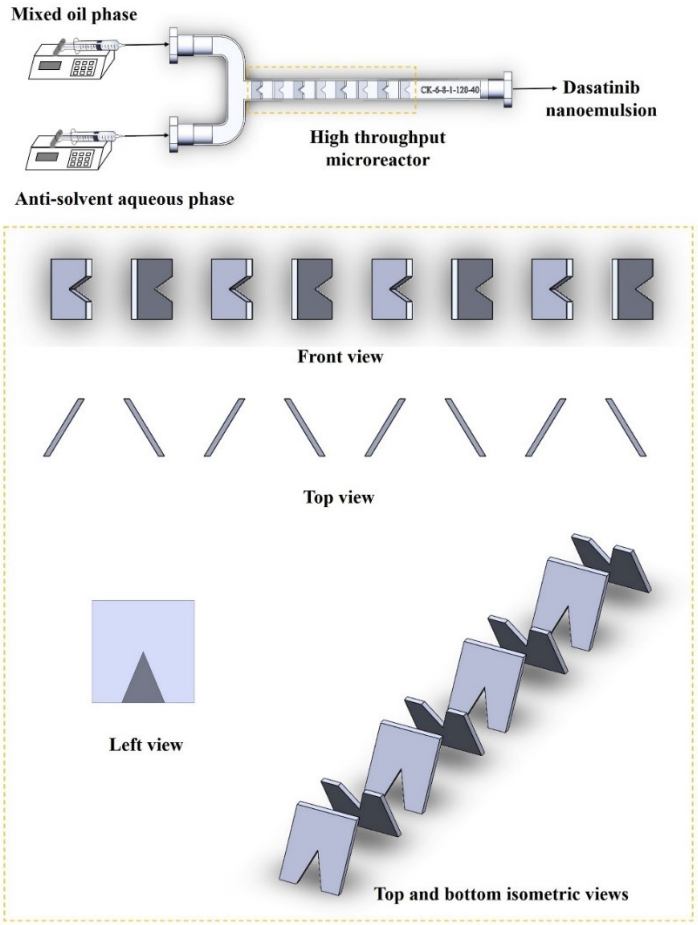

Fig. S1 Experimental device for the preparation process of dasatinib nanoemulsion.

Supporting Information 2: Particle size control model for Dassatinib nanoemulsion under microfluidic state

In a microreactor, it is easier to achieve sufficient mixing and contact between the mixed oil and water phases, resulting in the formation of nanoemulsions with small particle size and narrow particle size distribution. Combining the flow state of microfluids in microreactors with the preparation experiment of nanoemulsions, establishing a particle size control model for nanoemulsions will be beneficial for guiding the preparation of high-quality nanoemulsions. In this study, dimensional analysis method was adopted to establish a microfluidic particle size control model for dasatinib nanoemulsions. Through the analysis of the experimental process, it can be seen that there are six main influencing factors on the average diameter of nanoemulsion droplets (d_m), namely radius of the microreactor (R_m), fluid density (ρ), fluid viscosity (μ), interfacial tension coefficient (σ), total oil-water two-phase flow rate (Q), and oil-water two-phase flow rate ratio (q), as shown in Table S1. Therefore, the average diameter of nanoemulsion droplets can be abstractly represented by the following equation:

$$d_m = f(Rm, \rho, \mu, \sigma, Q, q) \quad (1)$$

Table S1 Factors influencing the average diameter of nanoemulsion droplets

Factors	Symbol	Unit	Dimension
Radius of microreactor	R_m	m	$[L]$
Oil phase density	ρ	$kg \cdot m^{-3}$	$[M \cdot L^{-3}]$
Oil phase viscosity	μ	$kg \cdot m^{-1} \cdot s^{-1}$	$[M \cdot L^{-1} \cdot T^{-1}]$
Interfacial tension coefficient	σ	$kg \cdot s^{-2}$	$[M \cdot T^{-2}]$
Total flow rate of the two-phases	Q	$m^3 \cdot s^{-1}$	$[L^3 \cdot T^{-1}]$
Flow rate ratio of oil phase to water phase	q	-	-

Among them, the basic physical dimensions include length [L], mass [M], and time [T], which are independent and cannot be derived from each other. Therefore, physical dimension of d_m can be represented by the exponential form of the three basic physical dimensions:

$$[d_m] = [L]^x[M]^y[T]^z \quad (2)$$

The principle of dimensional harmony and the π principle of fluid mechanics are combined to establish

corresponding physical models for solution. In this study, μ, ρ and R_m was selected as the three basic physical dimensions, and the other physical quantities were selected as the derived dimensions. Assuming the following equation holds:

$$f(d_m, Rm, \rho, \mu, \sigma, Q, q) = 0 \tag{3}$$

Then the process can be represented by a relationship expressed by (7-3=4) dimensionless π numbers, namely:

$$[\mu] = L^{-1}T^{-1}M^1 \tag{4}$$

$$[\rho] = L^{-3}T^0M^1 \tag{5}$$

$$[Rm] = L^1T^0M^0 \tag{6}$$

To ensure that μ, ρ and R_m is dimensionally independent of each other and cannot form dimensionless numbers. Therefore, it is required that their exponential product cannot be 0, namely the exponential determinant cannot be 0, as shown in the following equation:

$$\Delta = \begin{vmatrix} -1 & -1 & 1 \\ -3 & 0 & 1 \\ 1 & 0 & 0 \end{vmatrix} = -1 \neq 0 \tag{7}$$

From the above equation, it can be seen that the three basic dimensions selected are independent of each other. This dimensionless array can be represented as:

$$\pi_1 = \frac{d_m}{\mu^{\alpha_1}\rho^{\beta_1}Rm^{\gamma_1}}; \pi_2 = \frac{Q}{\mu^{\alpha_2}\rho^{\beta_2}Rm^{\gamma_2}}; \pi_3 = \frac{\sigma}{\mu^{\alpha_3}\rho^{\beta_3}Rm^{\gamma_3}}; \pi_4 = q \tag{8}$$

Among them α_i, β_j and γ_k represent the power coefficient of μ, ρ and R_m, where i, j, and k are natural numbers of 1-3, respectively.

According to the principle of dimensional harmony, it can be concluded that:

$$[\pi_1] = [L] = \left[L^{-1}T^{-1}M^1\right]^{\alpha_1}\left[L^{-3}T^0M^1\right]^{\beta_1}\left[L^1T^0M^0\right]^{\gamma_1} \tag{9}$$

After calculation, it can be concluded that:

$$\begin{cases} -\alpha_1 - 3\beta_1 + \gamma_1 = 1 \\ -\alpha_1 = 0 \\ \alpha_1 + \beta_1 = 0 \end{cases} \Rightarrow \begin{cases} \alpha_1 = 0 \\ \beta_1 = 0 \\ \gamma_1 = 1 \end{cases} \tag{10}$$

$$\pi_1 = \frac{d_m}{Rm}; \pi_2 = \frac{Q}{\mu\rho^{-1}Rm^2}; \pi_3 = \frac{\sigma}{\mu^2\rho^{-1}Rm^{-1}} \tag{11}$$

Therefore, Eq.3 can be transformed into the following equations:

$$\frac{d_{\mathrm{m}}}{R\mathrm{m}} = f\left(\frac{Q}{\mu\rho^{-1}R\mathrm{m}^{2}}, \frac{\sigma}{\mu^{2}\rho^{-1}R\mathrm{m}^{-1}}, q\right) \quad (12)$$

$$d_{\mathrm{m}} = Aq^{B}R\mathrm{m}\left(\frac{Q}{\mu\rho^{-1}R\mathrm{m}^{2}}\right)^{C}\left(\frac{\sigma}{\mu^{2}\rho^{-1}R\mathrm{m}^{-1}}\right)^{D} \quad (13)$$

where A, B, C, D are constant coefficients.

Based on the experimental results of preparing dasatinib nanoemulsion, as the dasatinib nanoemulsion system prepared in this section is already determined, encompassing known fluid density, viscosity, surface tension, and reactor radius, the primary focus is on investigating the influence of flow ratio and total flow rate on particle size. Consequently, Equation (13) can be simplified and transformed into Equation (14) as follows:

$$d_{\mathrm{m}} = Aq^{B}Q^{C} \quad (14)$$

By applying a logarithmic transformation with base e to the known experimental data, a data fitting process was conducted to predict the average droplet size of dasatinib in the internal phase of microemulsions, leading to the derivation of an empirical correlation Equation (15). The high R^2 value of 0.970 indicates a strong agreement between the model and experimental observations.

$$d_{\mathrm{m}}(\mathrm{nm}) = e^{4.33}q^{0.1121}Q^{0.1317} \quad (15)$$

To validate the precision of the empirical correlation, an error analysis was conducted.

Supporting Information 3: CFD simulations of liquid-liquid two-phase flow

SI 3.1 Control equations

The formation of dasatinib nanoemulsion is a typical liquid-liquid two-phase interaction process. The governing flow dynamics are encapsulated within a system of equations, comprising continuity equations and momentum balances, which are articulated as follows [5, 6]:

$$\nabla\vec{v}=0 \quad (16)$$

$$\frac{\rho\partial\vec{v}}{\partial t} + \rho\left(\vec{v}\cdot\nabla\right)\vec{v} + \nabla p - \eta\nabla^{2}\vec{v} - F = 0 \quad (17)$$

where $\vec{v}$ represents the velocity vector, ρ represents the fluid density, η represents the dynamic viscosity, and p represents the pressure. F represents surface tension between the two distinct phases, and it can be incorporated as a crucial parameter[5]:

$$F = \sigma\kappa(x, t)\nabla c \quad (18)$$

where σ represents surface tension coefficient, the κ denotes the unit normal vector to the surface at the interface where these two phases coexist.

The precise delineation and subsequent tracking of the interfaces separating various phases is facilitated by solving a continuity equation that pertains to the volume fraction of one (or multiple) of these phases. For a specific phase under consideration, this equation adopts the following explicit form:

$$\frac{1}{\rho_i}\left[\frac{\partial}{\partial t}\left(C_i\rho_i\right) + \nabla \cdot \left(C_i\rho_i\vec{v}_i\right)\right] = S_{C_i} + \sum_{i=1}^{n}\left(\dot{m}_{ij} - \dot{m}_{ji}\right) \quad (19)$$

where $\dot{m}_{ij}$ is the mass transfer form phase *i* to phase *j*, and $\dot{m}_{ji}$ is the mass transfer form phase *j* to phase *i*. S_{α_i} is 0 in this study.

SI 3.2 Simulation processes

In order to analyze the flow pattern of liquid-liquid two-phase flow in the high throughput microreactor with TNRB, CFD simulation method was adopted. The internal fluid domain of the high throughput microreactor was extracted as shown in Fig. S2(a). Due to the small flow velocity and Reynolds number less than 2000 during this experiments, the fluid was in a laminar flow state, therefore the laminar flow model was adopted. In this system, the oil phase and water phase were immiscible phases, and to obtain the interfacial area between fluids, the VOF model was adopted. The inlet of the two fluids was the velocity inlet, the outlet was the pressure outlet, and the geometric boundary was a non-slip wall surface. The fluid materials were mixed oil and ultrapure water, and their physical property parameters were shown in Table S2.

Table S2 Physical property parameters of oil-water two-phase flow

Phases	Materials	Density (kg/m^3)	Viscosity ($kg/(m \cdot s)$)	Interfacial tension (mN/m)
Disperse phase	Mixed oil	973	0.0178	1.44
Continuous phase	Ultrapure water	998.2	0.001003	

SI 3.3 Evaluation method

In the context of liquid-liquid biphasic processes, the inherent immiscibility between the fluids poses challenges for accurate quantification. As shown in Fig. S2(b), the high throughput microreactor with FNBS introduces a high degree of complexity, resulting in a chaotic two-phase interface that eludes direct calculation. The specific surface area ratio emerges as a more suitable metric for assessing such complex

structures [7]. It offers a versatile approach that can effectively capture the intricacies of the biphasic interface, overcoming the limitations encountered with traditional methods in the face of mixers characterized by FNBS and non-ideal flow conditions.

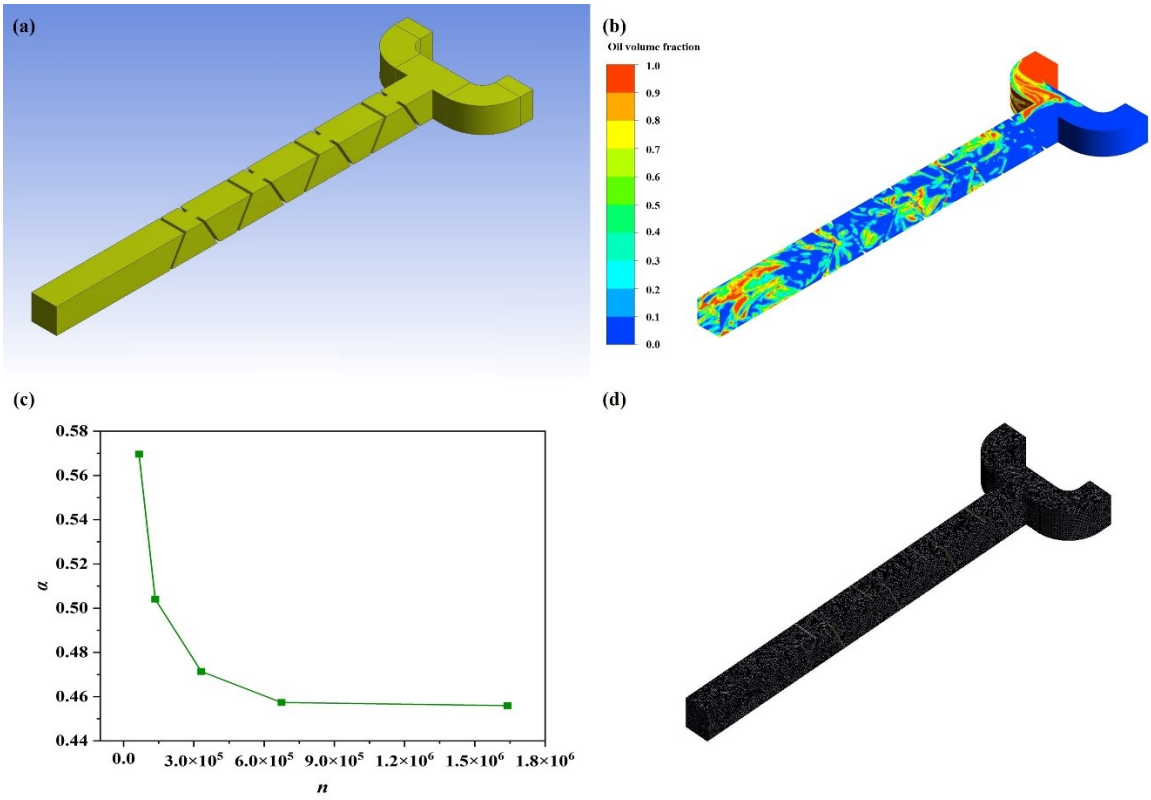

Fig. S2 CFD simulations of the high throughput microreactor: (a) internal fluid domain, (b) volume fraction distribution of oil phase in the wall, (c) effects of grid count on the specific surface area ratio at the outlet, (d) optimal grid distribution

To delineate the interfacial dynamics between the two phases, we employed the specific surface area ratio (α) as a metric within the system. This ratio is formulated as follows, providing a quantitative representation of the interaction [7]:

$$\alpha = \frac{A_s}{V} \tag{20}$$

where A_s denotes the aggregate surface area of the interface separating the two phases, and V represents the combined volume occupied by these phases.

The ratio of specific surface area within a radial section of length L can be mathematically expressed as follows, offering a quantitative analysis of the interfacial characteristics along this particular dimension:

$$\alpha = \frac{\int_0^L A_i dL}{\int_0^L A dL} \tag{21}$$

where A_i represents the interfacial area between the two fluids within that section, and A denotes the total area of the radial section itself.

The aggregate specific surface area ratio across multiple radial planes is formulated as follows:

$$\bar{\alpha} = \frac{\sum_{1}^{n} \alpha_{l_i}}{n} \tag{22}$$

where α_{l_i} signifies the ratio at individual planes, and n represents the total count of these sections. This averaged metric offers a comprehensive insight into the interfacial properties spanning the examined radial planes.

SI3.4 Mesh independence analyses

To conserve computational time while maintaining other parameters constant, a study on mesh independence for the structural model was conducted using various grid sizes at a higher flow velocity. The oil-to-water velocity ratio was set at 1:3, with oil phase velocity at 0.417 m/s and water phase velocity at 1.25 m/s. To evaluate mesh independence in the liquid-liquid heterogeneous dispersion process, the specific surface area ratio at the outlet cross-section of the microflow reactor was utilized as the criterion. Five distinct grid counts were chosen, spanning from 65,000 to 1,640,000, corresponding to grid sizes of 1.3mm, 1.0mm, 0.7mm, 0.5mm, and 0.35mm, respectively. Simulation results are depicted in Fig. S2(c). As observed, the specific surface area ratio at the outlet decreases with increasing grid count, stabilizing at a sufficiently large grid number, indicating that a grid count of 670,000 (specifically 674,567 grids with a 0.5mm size) meets the required computational accuracy. Consequently, a 0.5mm grid size was selected for subsequent simulation studies (Fig. S2(d)).

Supporting Information 4: Liquid-liquid two-phase flow behavior in high-throughput microreactor

To investigate the influence of total flow rate and flow ratio on the two-phase flow behavior in the high-throughput microreactor, the flow rates of the oil and water phases were adjusted based on the emulsification experimental requirements. CFD numerical simulations were conducted, using average specific surface area as the evaluation metric, and the results are presented in Fig. S3. As shown in Fig. S3(a), the specific surface area increases with the flow ratio, indicating improved two-phase dispersion. The mass distribution contour plots, with blue representing the aqueous phase and red the mixed oil phase, reveal that at lower flow ratios,

fewer and smaller droplets are present (Fig. S3(c)). As the flow ratio increases, droplet formation intensifies, although the specific surface areas at ratios of 1:3 and 1:5 are comparable, with the former exhibiting a secondary droplet. The flow field structure facilitates better shearing of the oil phase by the aqueous phase, leading to more uniform dispersion and smaller droplet sizes (i.e., increased specific surface area). This suggests that a flow ratio of 1:3 holds potential for producing uniform dasatinib nanoemulsions with smaller particle sizes.

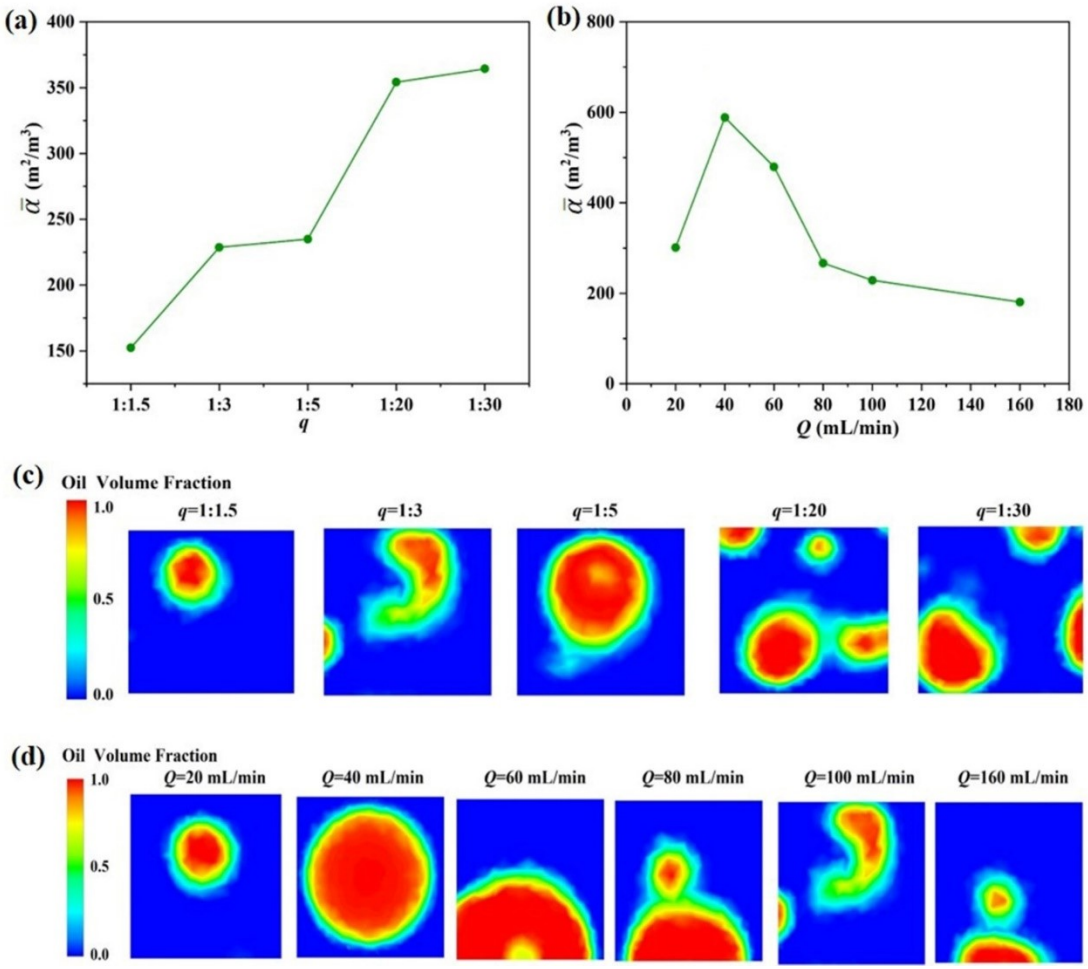

Fig. S3 Effects of the flow ratio and the total flow rate on the average specific surface area and liquid-liquid two-phase flow behavior: (a) and (c) flow ratio, (b) and (d) total flow rate

At a flow ratio of 1:3, the total flow rate range was expanded, and the simulation results and contour plots are depicted in Fig. S3(b) and 4(d). At lower total flow rates, fluid dispersion primarily relies on spontaneous mechanisms due to reduced flow velocities. When the flow rate reaches 40mL/min, the maximum specific surface area is achieved, indicating optimal contact and shearing between the oil and water phases to form droplets. Further increases in flow rate lead to faster convergence in simulations due to higher velocities, resulting in a gradual decrease in the average specific surface area. At a total flow rate of 40mL/min, the oil-water interface near the outlet's radial cross-section is substantial, effectively promoting the formation of oil-

in-water droplets.

Supporting Information 5: Particle size of nanoemulsions prepared by three methods

Table S3 Particle size of nanoemulsions prepared by three methods

Method	*t* (s)	Average size (nm)	PDI
Traditional batch method	300	430.3	0.548
	600	284.3	0.899
	1800	128.8	0.917
Microreactor (1mm)	0.23	45.1	0.390
High-throughput microreactor	22.5	18.8	0.300

Supporting Information 6: Particle size distribution data of dasatinib nanoemulsion

Table S4 Nanoemulsion particle size and PDI size measured under different oil phases

Oil phase	Size (nm)	PDI
Triacetin	172.6	0.45
Ethyl oleate	133.4	0.29
Epoxidized soybean oil	1002	0.49
Oleic acid	447.5	0.42

Table S5 Nanoemulsion particle size and PDI size measured with different co emulsifiers

Co-emulsifier	Size (nm)	PDI
Ethylene glycol	559.4	0.47
Glycerol	1049	0.74
Ethanol	447.5	0.42

Table S6 Nanoemulsion particle size and PDI size measured with different emulsifiers

Emulsifier	Size (nm)	PDI
Tween-20	447.5	0.42

RH-40	18.79	0.30	

Table S7 Particle size determination results with different flow ratios

q	Q_{oil} (mL/min)	Q_{H_2O} (mL/min)	Size (nm)	Intensity (%)	PDI
1:1.5	40	60	20.74	74.3	0.44
1:3	25	75	22.06	75.5	0.44
1:5	16.7	83.3	21.01	77.8	0.41
1:20	4.76	95.24	17.36	79.5	0.35
1:30	3.23	96.77	13.59	79.8	0.12

Table S8 Particle size determination results of different flow rates

Q (mL/min)	Q_{oil} (mL/min)	Q_{H_2O} (mL/min)	Size (nm)	Intensity (%)	PDI
20	5	15	23.61	79.2	0.39
40	10	30	18.79	85.9	0.30
60	15	45	18.96	82.3	0.32
80	20	60	21.05	77.7	0.42
100	25	75	22.06	75.5	0.44
160	40	120	22.18	64.4	0.53

References

1. H. R. Wu, C. Q. Wang, J. X. Wang, J. F. Chen and Y. Le, *International Journal of Nanomedicine*, 2020, **15**, 2391-2402.
2. J. Riewe, P. Erfle, S. Melzig, A. Kwade, A. Dietzel and H. Bunjes, *International Journal of Pharmaceutics*, 2020, **579**, 119167.
3. A. Larrea, A. Clemente, E. Luque-Michel and V. Sebastian, *Chemical Engineering Journal*, 2017, **316**, 663-672.
4. P. Yu, S. Zhao, Y. Nie, Y. Wei, R. Hu, W. He, N. Zhu, Y. Li, D. Ji and K. Guo, *Numerical Heat Transfer, Part A: Applications*, 1-20.
5. Q. Yu and X. Chen, *Journal of the Brazilian Society of Mechanical Sciences and Engineering*, 2023, **45**, 571.
6. E. A. Wenzel, F. A. Kulacki and S. C. Garrick, *International Journal of Heat and Mass Transfer*, 2016, **97**, 653-661.
7. S. Zhao, Y. Nie, Y. Wei, P. Yu, W. He, N. Zhu, Y. Li, D. Ji and K. Guo, *International Journal of Chemical Reactor Engineering*, 2022.